**Astronomy
&
Astrophysics**

The 2–10 keV luminosity as a Star Formation Rate indicator

P. Ranalli[1], A. Comastri[2], and G. Setti[1]

[1] Dipartimento di Astronomia, Università di Bologna, via Ranzani 1, 40127 Bologna, Italy
[2] INAF – Osservatorio Astronomico di Bologna, via Ranzani 1, 40127 Bologna, Italy

Abstract. Radio and far infrared luminosities of star-forming galaxies follow a tight linear relation. Making use of ASCA and BeppoSAX observations of a well-defined sample of nearby star-forming galaxies, we argue that tight linear relations hold between the X-ray, radio and far infrared luminosities. The effect of intrinsic absorption is investigated taking NGC 3256 as a test case. It is suggested that the hard X-ray emission is directly related to the Star Formation Rate. Star formation processes may also account for most of the 2–10 keV emission from LLAGNs of lower X-ray luminosities (for the same *FIR* and radio luminosity). Deep *Chandra* observations of a sample of radio-selected star-forming galaxies in the Hubble Deep Field North show that the same relation holds also at high ($0.2 \lesssim z \lesssim 1.3$) redshift. The X-ray/radio relations also allow a derivation of X-ray number counts up to very faint fluxes from the radio Log N–Log S, which is consistent with current limits and models. Thus the contribution of star-forming galaxies to the X-ray background can be estimated.

Key words. X-rays: galaxies – radio continuum: galaxies – galaxies: high-redshift – infrared: galaxies – galaxies: fundamental parameters – galaxies: starburst

1. Introduction

Radio continuum and far infrared (*FIR*) luminosities of star-forming galaxies are known to show a *tight linear* relationship spanning four orders of magnitude in luminosity (van der Kruit 1973; De Jong et al. 1985; Condon 1992) and up to a redshift ∼1.3 (Garrett 2002). This is interpreted as due to the presence of massive, young stars embedded in dust: a fraction of their UV radiation is absorbed by dust grains and reradiated in the infrared band, while supernova explosions may accelerate the electrons producing at radio wavelengths the observed synchrotron emission (Harwit & Pacini 1975; Helou et al. 1985). Since massive ($M \gtrsim 5\ M_\odot$) stars are short-lived, these luminosities are assumed to be indicators of the global Star Formation Rate (*SFR*) in a galaxy. Following Condon (1992) and Kennicutt (1998), the relation between *SFR* (referred to stars with $M > 5\ M_\odot$) and radio/*FIR* luminosities can be written as:

$$SFR = \frac{L_{1.4\ \mathrm{GHz}}}{4.0 \times 10^{28}}\ M_\odot/\mathrm{yr} \qquad (1)$$

$$SFR = \frac{L_{FIR}}{2.2 \times 10^{43}}\ M_\odot/\mathrm{yr} \qquad (2)$$

with the *FIR* flux defined after Helou et al. (1985) as:

$$FIR = 1.26 \times 10^{-11}(2.58 S_{60\mu} + S_{100\mu})\ \mathrm{erg\ s^{-1}\ cm^{-2}} \qquad (3)$$

where $L_{1.4\ \mathrm{GHz}}$ is in $\mathrm{erg\ s^{-1}\ Hz^{-1}}$, L_{FIR} in $\mathrm{erg\ s^{-1}}$ and infrared fluxes are in Jy.

Star-forming galaxies are also luminous sources of X-ray emission, due to a number of High Mass X-ray Binaries (HMXB), young supernova remnants, and hot plasmas associated to star-forming regions and galactic winds (Fabbiano 1989). A non linear ($L_X \propto L_{FIR}^{0.6}$) and much scattered (dispersion of about 2 dex) relation was found between *FIR* and soft (0.5–3.0 keV) X-ray luminosities of IRAS-bright and/or interacting/peculiar galaxies measured by the *Einstein* satellite (Griffiths & Padovani 1990). A somewhat different result was found by David et al. (1992), i.e. a linear relation between *FIR* and 0.5–4.5 keV luminosities for a sample of starburst galaxies observed by *Einstein*. A large number of upper limits to the X-ray flux (12 upper limits vs. 11 detections for Griffiths & Padovani 1990) along with high uncertainties in the X-ray and *FIR* fluxes may explain this discrepancy. Moreover, these studies suffered by the lack of knowledge about spectral shapes and internal absorption in star forming galaxies caused by the limited sensitivity and spectral capabilities of the IPC detector onboard *Einstein*.

Here, with the high sensitivity and the broad-band spectral capabilities of the ASCA and BeppoSAX satellites, we extend these studies to the 2–10 keV band which is essentially free from absorption. In the following paragraphs a sample of nearby star forming galaxies is assembled (Sect. 2) and linear relations among radio, *FIR* and both soft and hard X-ray luminosities are found (Sect. 3). Possible biases are discussed and the use of X-ray luminosities as a *SFR* indicator is proposed (Sect. 4). In Sect. 5 we present a study of star-forming galaxies in the Hubble Deep Field North and test the

validity of the X-ray SFR law. Implications for the contribution of star-forming galaxies to the X-ray counts and background are discussed in Sect. 6.

Throughout this paper, we assume $H_0 = 50$ and $q_0 = 0.1$.

2. The local sample

The atlas of optical nuclear spectra by Ho et al. (1997) (hereafter HFS97) represents a complete spectroscopic survey of galaxies in the Revised Shapley-Ames Catalog of Bright Galaxies (RSA; Sandage & Tammann 1981) and in the Second Reference Catalogue of bright galaxies (RC2; de Vaucouleurs et al. 1976) with declination $\delta > 0°$ and magnitude $B_T < 12.5$. Optical spectra are classified in HFS97 on the basis of line intensity ratios according to Veilleux & Osterbrock (1987); galaxies with nuclear line ratios typical of star-forming systems are labeled as "H II nuclei". This sample of H II galaxies contains only spirals and irregulars from Sa to later types, except for a few S0 which were excluded from our analysis since their properties resemble more those of elliptical galaxies.

A cross-correlation of the HFS97 sample with the ASCA archive gives 18 galaxies clearly detected in the 2–10 keV band with the GIS instruments. Four additional objects in the field of view of ASCA observations were not detected: the 2–10 keV flux upper limits are too loose to add any significant information, and thus we did not include them in the sample. The cross-correlation of the HFS97 sample with the BeppoSAX archive does not increase the number of detections. When a galaxy was observed by both satellites, we chose the observation with better quality data.

Far infrared fluxes at 60 μ and 100 μ were taken from the IRAS Revised Bright Galaxy Sample (RBGS, Mazzarella et al., in preparation) which is a reprocessing of the final IRAS archive with latest calibrations. While the RBGS measurements should be more accurate, we checked that the use of the older catalogue of IRAS observations of large optical galaxies[1] by Rice et al. (1988), coupled with the Faint Source Catalogue (FSC, Moshir et al. 1989) for smaller galaxies, does not significantly change our statistical analysis. FIR fluxes for NGC 4449 were taken from Rush et al. (1993). Radio (1.4 GHz) fluxes were obtained from the Condon et al. (1990, 1996) catalogues (except for NGC 4449, taken from Haynes et al. 1975). Distances were taken from Tully (1988) and corrected for the adopted cosmology.

Part of the X-ray data have already been published; in the cases where published data were not available in a form suitable for our analysis, the original data were retrieved from the archive and reduced following standard procedures and with the latest available calibrations. Images and spectra were extracted from the pipeline-screened event files. The images were checked against optical (Digital Sky Survey) and, where available, radio (1.4 GHz) images in order to look for possible source confusions. Fluxes were calculated in the 0.5–2.0 and 2–10 keV bands from best-fit spectra for the GIS2 and GIS3 instruments and corrected for Galactic absorption only. The uncertainty on the fluxes is of the order of 10%. Depending on the

quality of data, the best-fit spectrum is usually represented by a two-component model with a thermal plasma plus a power-law or just a power-law.

The galaxy IC 342 has shown some variability, mainly due to a burst in 1993 of an ultraluminous X-ray binary. M 82 is also a variable source. For each galaxy we summarize in the Appendix the results from several X-ray observations and estimate a time-averaged luminosity.

One object (M 33) was not included in the sample since its broad-band (0.5–10 keV) X-ray nuclear spectrum is dominated by a strong variable source (M 33 X-8) identified as a black hole candidate (Parmar et al. 2001).

Therefore, our sample (hereafter local sample) consists of the 17 galaxies listed in Table 1. Since it is not complete in a strict sense due to the X-ray selection, we have checked for its representativeness with reference to the SFR. The median SFR values for HFS97 is $SFR_{med} \sim 1.65$ $M_\odot$/yr. Considering objects with $SFR > SFR_{med}$ there are 14 galaxies in the local sample out of 98 in HFS97 (14%), while there are 3 objects with $SFR < SFR_{med}$ (3%). Thus the high luminosity tail is better sampled than the low luminosity one.

We also include data for 6 other well-known starburst galaxies which were not in the HFS97 survey because they are in the southern emisphere. On the basis of their line intensity ratios[2] they should be classified as H II nuclei. In Table 1 we label them as supplementary sample.

3. The radio/FIR/X-rays correlation

As a preliminary test, we perform a least-squares analysis for the well-known radio/FIR correlation, which yields

$$\text{Log}(L_{FIR}) = (0.98 \pm 0.06) \, \text{Log}(L_{1.4}) + 15.4 \pm 1.6. \qquad (4)$$

The dispersion around the best-fit relation is given as the estimate s of the standard deviation σ:

$$s = \frac{1}{N - \nu} \cdot \sqrt{\sum \left(\text{Log } L_{obs} - \text{Log } L_{pred} \right)^2} \qquad (5)$$

where ν is the number of free parameters, N is the number of points in the fit, L_{pred} is the luminosity expected from the best fit relation and L_{obs} the observed one. For the radio/FIR correlation (Eq. (4)) we find $s = 0.18$.

Following Helou et al. (1985) we also calculate the mean ratio q between the logarithms of FIR and radio fluxes, obtaining $q \simeq 2.2 \pm 0.2$. This value is consistent with the mean $q = 2.34 \pm 0.01$ for the 1809 galaxies in the IRAS 2 Jy sample by Yun et al. (2001).

Soft X-rays

A test for the soft X-ray/FIR/radio relations (Fig. 1) yields

$$\text{Log}(L_{0.5-2}) = (0.87 \pm 0.08) \, \text{Log}(L_{FIR}) + 2.0 \pm 3.7 \qquad (6)$$

$$\text{Log}(L_{0.5-2}) = (0.88 \pm 0.08) \, \text{Log}(L_{1.4}) + 14.6 \pm 2.2 \qquad (7)$$

with $s \simeq 0.26$ and 0.24 respectively.

---

[1] Blue-light isophotal major diameter (D_{25}) greater than 8′.

[2] References: NGC 55 – Webster & Smith (1983); NGC 253, 1672 & 1808 – Kewley et al. (2001); NGC 3256 – Moran et al. (1999); Antennae – Rubin et al. (1970), Dobrodiy & Pronik (1979).

Table 1. Data for galaxies in our local samples. All galaxies were observed with ASCA, except those marked with * observed by BeppoSAX. Distances in Mpc; X-ray fluxes in 10^{-13} erg s^{-1} cm^{-2}, *FIR* fluxes in 10^{-9} erg s^{-1} cm^{-2} and radio fluxes in Jy; X-ray luminosities in 10^{40} erg s^{-1}, *FIR* luminosities in 10^{43} erg s^{-1} and radio luminosities in 10^{29} erg s^{-1} Hz^{-1}. The uncertainty on fluxes and luminosities is of the order of 10%. References: 1. Cappi et al. (1999); 2. Della Ceca et al. (1996); 3. Della Ceca et al. (1999); 4. Zezas et al. (1998); 5. Della Ceca et al. (1997); 6. Dahlem et al. (1998); 7. Moran et al. (1999); 8. Sansom et al. (1996).

GALAXY	D	$F_{0.5-2}$	$L_{0.5-2}$	F_{2-10}	L_{2-10}	F_{FIR}	L_{FIR}	$F_{1.4}$	$L_{1.4}$	Refs.
FLUXES AND LUMINOSITIES: MAIN SAMPLE										
M 82*	7.8	97	7.1	290	21	67	49	7.7	5.6	1
M 101	8.1	5.4	0.42	6.8	0.54	6.0	4.7	0.75	0.59	this work
M 108	21	4.4	2.3	6.0	3.2	2.0	11	0.31	1.63	this work
NGC 891	14	8.3	2.1	19	4.8	4.5	11	0.70	1.74	this work
NGC 1569	2.4	5.4	0.037	2.2	0.015	2.5	0.17	0.41	0.028	2
NGC 2146	26	8.2	6.5	11	9.0	7.3	59	1.1	8.7	3
NGC 2276	55	2.1	7.6	4.4	16	0.85	31	0.28	10	this work
NGC 2403	6.3	16	0.77	9.3	0.44	2.7	1.3	0.33	0.16	this work
NGC 2903	9.4	7.9	0.84	7.0	0.74	3.7	4.0	0.41	0.43	this work
NGC 3310	28	7.4	6.9	2.1	2.0	1.7	16	0.38	3.6	4
NGC 3367	64	1.8	8.7	1.6	7.9	0.38	19	0.10	4.9	this work
NGC 3690	69	5.7	33	11	62	5.3	310	0.66	38	4
NGC 4449	4.5	8.3	0.20	4.8	0.12	1.9	0.47	0.6	0.1	5
NGC 4631	10	9.4	1.2	9.3	1.2	4.9	6.2	1.2	1.5	6
NGC 4654	25	0.6	0.4	0.9	0.66	0.93	7.1	0.12	0.89	this work
NGC 6946	8.2	30	2.5	12	0.97	7.9	6.4	1.4	1.1	this work
IC 342	5.9	18	0.73	110	4.4	11	4.4	2.3	0.92	this work
SUPPLEMENTARY SAMPLE										
NGC 55	1.9	18	0.082	6.8	0.031	4.7	0.21	0.38	0.017	6
NGC 253*	4.5	25	0.59	50	1.2	49	12	5.6	1.3	1
NGC 1672	22	5.8	3.2	6.1	3.4	2.3	13	0.45	2.5	this work
NGC 1808	16	6.5	2.0	7.6	2.4	5.3	17	0.52	1.6	this work
NGC 3256	56	9.0	34	6.2	23	4.8	180	0.66	25	7
Antennae	38	7.2	13	5.3	9.2	2.6	45	0.57	9.9	8

Our result is consistent with the $L_{0.5-4.5} \propto L_{FIR}^{0.95\pm0.06}$ relation found by David et al. (1992) for normal and starburst galaxies from the IRAS Bright Galaxy Sample, but it is only marginally consistent with the much flatter and more dispersed relationship obtained by Griffiths & Padovani (1990) for a sample of IRAS selected galaxies ($L_{0.5-3 \, keV} \propto L_{60 \, \mu}^{0.62\pm0.14}$) and for a sample of starburst/interacting galaxies ($L_{0.5-3 \, keV} \propto L_{60 \, \mu}^{0.70\pm0.12}$).

The inclusion of the objects of the supplementary sample (Table 1) does not significantly change the slopes, i.e. $L_{0.5-2.0 \, keV} \propto L_{FIR}^{0.88\pm0.07}$; likewise, if we use the $60 \, \mu$ luminosity instead of *FIR*, we obtain $L_{0.5-2.0 \, keV} \propto L_{60 \, \mu}^{0.85\pm0.07}$.

By assuming an exactly linear slope, the best fit relations for the local (local+supplementary) sample become:

$$\mathrm{Log}(L_{0.5-2}) = \mathrm{Log}(L_{FIR}) - 3.68 \; (3.70) \tag{8}$$

$$\mathrm{Log}(L_{0.5-2}) = \mathrm{Log}(L_{1.4}) + 11.08 \; (11.10) \tag{9}$$

with $s \simeq 0.27$ and 0.24 respectively.

By applying an F-test we find that the free-slope fits are not significantly better than those with the linear slope, the improvement being significant only at the 1σ level.

Hard X-rays

In Fig. 2 we plot 2–10 keV luminosities versus *FIR* and radio ones. Least-squares fits yield:

$$\mathrm{Log}(L_{2-10}) = (1.08 \pm 0.09) \, \mathrm{Log}(L_{FIR}) - 7.1 \pm 4.2 \tag{10}$$

$$\mathrm{Log}(L_{2-10}) = (1.08 \pm 0.09) \, \mathrm{Log}(L_{1.4}) + 8.8 \pm 2.7 \tag{11}$$

with $s \simeq 0.30$ and 0.29 respectively. The linearity and the dispersion are not significantly changed neither by the inclusion of the supplementary sample ($L_{2-10} \propto L_{FIR}^{1.04\pm0.07}$ and $L_{2-10} \propto L_{1.4}^{1.01\pm0.07}$, $s \simeq 0.27$ and 0.26 respectively), nor by the use of the $60 \, \mu$ luminosity ($L_{2-10} \propto L_{60 \, \mu}^{1.01\pm0.07}$).

By assuming an exactly linear slope, the best fit relations for the local (local+supplementary) sample become:

$$\mathrm{Log}(L_{2-10}) = \mathrm{Log}(L_{FIR}) - 3.62 \; (3.68) \tag{12}$$

$$\mathrm{Log}(L_{2-10}) = \mathrm{Log}(L_{1.4}) + 11.13 \; (11.12) \tag{13}$$

with $s \simeq 0.29$ for both fits. There is no significant improvement (less than 1σ) in the free-slope fits with respect to the linear slope ones.

4. X-rays and the Star Formation Rate

The existence of a tight linear relation implies that the three considered bands all carry the same information. Since the
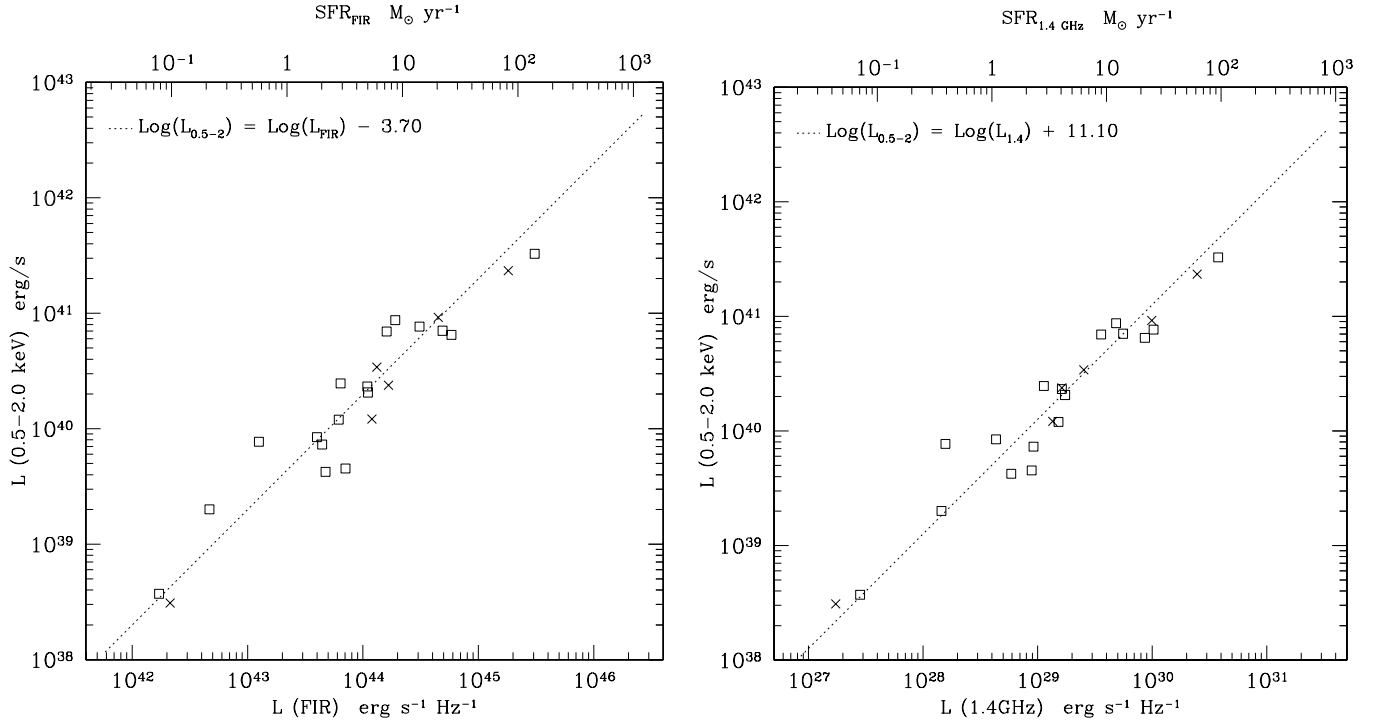
Fig. 1. The 0.5–2.0 keV luminosity of local star-forming galaxies vs. radio and *FIR* ones. Squares: local sample; crosses: supplementary sample; dotted lines: Eqs. (8), (9).
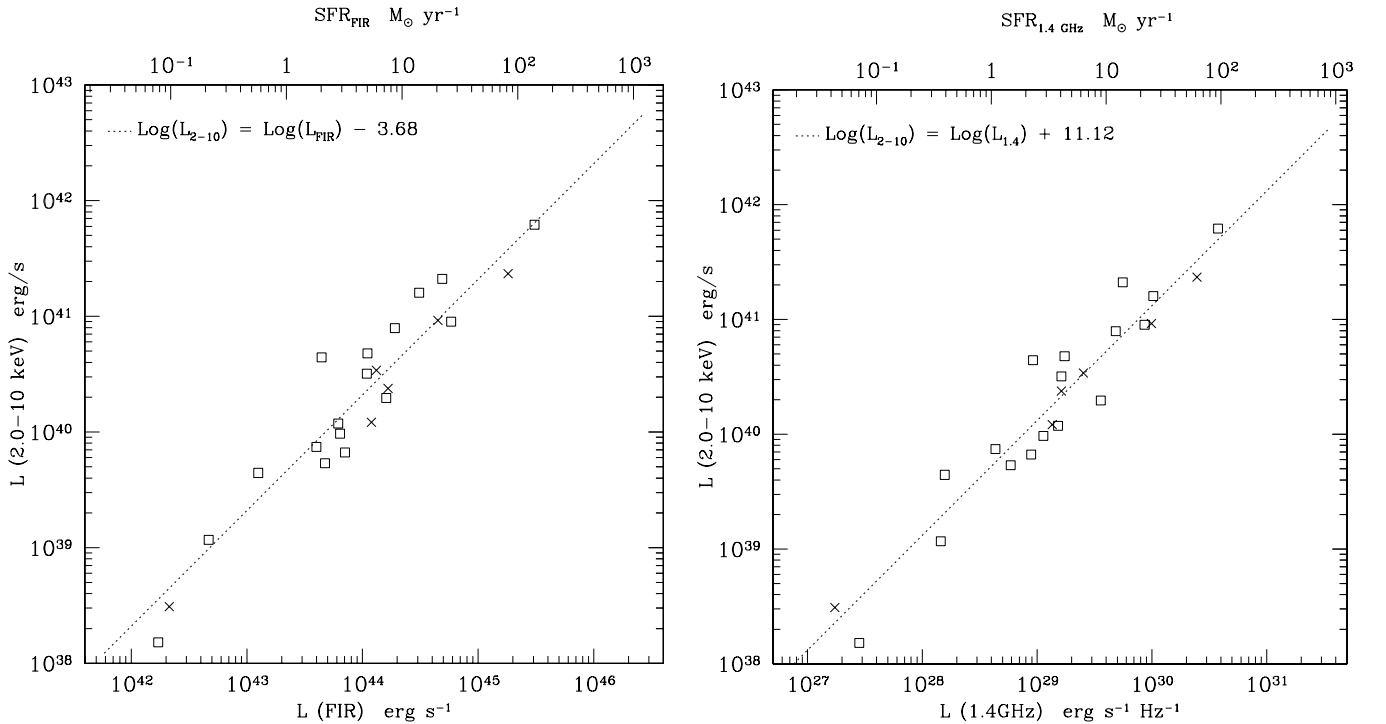

Fig. 2. The 2.0–10 keV luminosity of local star-forming galaxies vs. radio and *FIR* ones. Symbols as in Fig. 1; dotted lines: Eqs. (12), (13).

radio and far infrared luminosities are indicators of the *S FR*, the 0.5–2 keV and 2–10 keV luminosities should also be *S FR* indicators. However, before attempting to calibrate such relationships, we should consider the possible existence of selection effects.

Ho et al. (1995) made a special effort in obtaining *nuclear* nebular spectra, so that a reliable spectral classification

of the central engine could be derived. The main concern is the possibility that the H ɪɪ galaxies in the HFS97 sample could host a Low Luminosity AGN (LLAGN), which might significantly contribute to the overall energy output. To check for this possibility, Ulvestad & Ho (2002) observed with the VLA at 1.4 GHz a complete sample of 40 Sc galaxies in HFS97 with H ɪɪ spectra and did not find any compact luminous radio
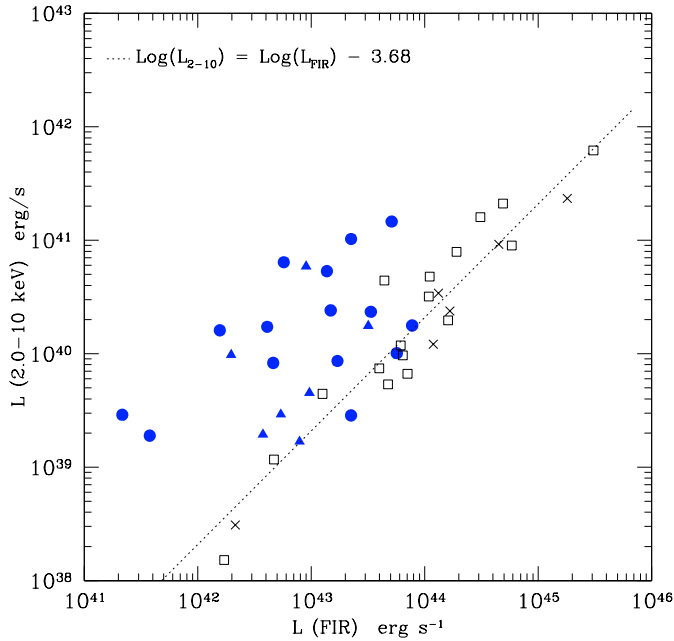
Fig. 3. 2.0–10 keV vs. *FIR* luminosities of star-forming galaxies and LLAGN. Filled triangles: LINERs, filled circles: Seyfert galaxies. Open symbols as in Fig. 1; line: Eq. (12).

Table 2. Identification of candidate star-forming galaxies in the Richards et al. (1998) catalogues with their X-ray counterpart (Brandt et al. 2001). The entry number in the *Chandra* catalogue is shown in parenthesis.

CHANDRA	VLA
CXOHDFN J123634.4+621212 (134)	3634+1212
CXOHDFN J123634.5+621241 (136)	3634+1240
CXOHDFN J123637.0+621134 (148)	3637+1135
CXOHDFN J123651.1+621030 (188)	3651+1030
CXOHDFN J123653.4+621139 (194)	3653+1139
CXOHDFN J123708.3+621055 (246)	3708+1056
CXOHDFN J123716.3+621512 (278)	3716+1512

LLAGN have a compact nucleus dominating the X-ray emission, while in the remaining objects off-nuclear sources and diffuse emission significantly contribute to the overall emission.

Following this investigation, we have analyzed the relations between radio/*FIR*/X-ray luminosities for the spiral galaxies in the Terashima et al. (2002) sample of LLAGN, drawn from HFS97 and observed with ASCA, comprising 7 LINERs and 15 Seyfert's with $4 \times 10^{39} \lesssim L_{2-10} \lesssim 5 \times 10^{41}$ erg s^{-1}. We find that the X-ray/*FIR* and X-ray/radio luminosity ratios generally exceed those of star-forming galaxies, but about one third of the objects have ratios falling on the same *locus* of the star-forming galaxies (Fig. 3). Therefore, the nuclear X-ray emission of these last LLAGN must be comparable to or weaker than the emission from star formation related processes. Moreover, the infrared (IRAS band) colours of these objects are also similar to those of star-forming galaxies, and completely different from those of QSOs, thus suggesting that the *FIR* luminosities of LLAGN may be powered by star formation.

5. Star-forming galaxies in the Hubble Deep Field

The 1 Ms *Chandra* (Brandt et al. 2001) and the radio (8.4 GHz: Richards et al. 1998; 1.4 GHz: Richards 2000 and Garrett 2000) catalogues of the Hubble Deep Field North (HDFN) reach a limiting flux which is deep enough to detect star-forming galaxies at redshifts up to $z \sim 1.3$, and can be used to check whether the radio/X-ray relation holds also for distant galaxies.

We searched for X-ray counterparts of radio sources in the the Richards et al. (1998) catalogue which contains optical and IR identifications allowing the selection of candidate star-forming galaxies. Our selection criterium has been to include all galaxies with Spiral or Irregular morphologies, known redshifts and no AGN signatures in their spectra (from Richards et al. 1998 or Cohen et al. 2000).

The mean positional uncertainties of both *Chandra* (for on-axis sources) and the VLA are ~0.3″, which added in quadrature give ~0.5″. Using this value as the encircling radius for coordinate matching 5 galaxies are found. However, there are two effects that can increase this value:

1. the shape and width of the *Chandra* PSF strongly depend on the off-axis and azimutal angles. Since the 1 Ms HDFN data consist of 12 observations with different pointing directions and position angles, there is no unique PSF model even for near on-axis sources;
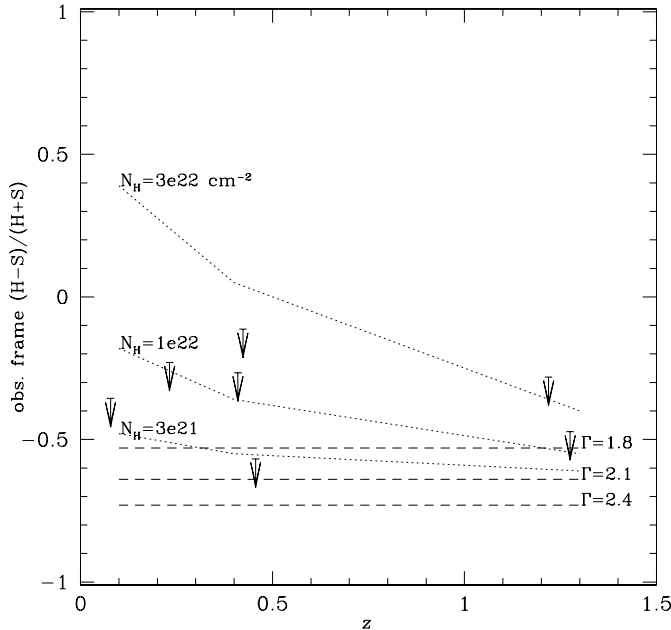
core. Instead, they found that the radio powers and morphologies are consistent with star formation processes rather than by accretion onto massive black holes; thus they suggest that H II nuclei intrinsically lack AGN. Therefore we believe that the HFS97 classification is reliable and that our sample is not polluted by AGN.

It is also worth noticing that the soft X-rays relationships may involve some further uncertainties related to the possible presence of intrinsic absorption (negligible in the 2–10 keV band for column densities usually found in normal galaxies). An example of this effect is the southern nucleus of NGC 3256 (see the Appendix), a dusty luminous merger remnant with two bright radio-IR cores where star formation is ongoing: while both of them fall on the radio/hard X-ray relation, only the northern core is on the radio/soft X-ray relation because the southern one lies behind a dust lane which absorbes at all wavelengths from ~1 μ to ~2 keV. The quasi-linearity of the soft X-ray relations suggests that absorption is unlikely to be relevant for the majority of the objects in our sample; however this effect may become significant at cosmological distances ($z \gtrsim 1-2$) where galaxies have more dust and gas at their disposal to form stars.

Thus we feel confident to propose the use of X-ray luminosities as *SFR* indicators. From Eqs. (8), (9), (12), (13) we derive:

$$SFR = 2.2 \times 10^{-40} L_{0.5-2 \text{ keV}} \qquad M_\odot/\text{yr} \qquad (14)$$

$$SFR = 2.0 \times 10^{-40} L_{2-10 \text{ keV}} \qquad M_\odot/\text{yr}. \qquad (15)$$

We also notice that there is growing evidence that star formation could play a major role even among those objects classified as LLAGN. The preliminary results of the *Chandra* LLAGN survey (Ho et al. 2001) show that only about one third of

Fig. 4. Observer's-frame hardness ratios for galaxies in the HDFN; there are only upper limits since none is detected in the 2–8 keV band (Brandt et al. 2001). The dotted lines show the *loci* for power-law spectra with slope $\Gamma = 2.1$ and different intrinsic rest-frame absorption; the dashed lines are for spectra of different slopes and no intrinsic absorption.

2. a displacement of several kpc between the brightest radio and X-ray positions, induced e.g. by an ultraluminous X-ray binary placed in a spiral arm and dominating the X-ray emission.

Thus, by making cross-correlations with increasing encircling radii we found that the number of coincidences increases up to a radius of $1.0''$ (which yields 7 matchings). There are no further coincidences up to a radius of several arcsecs, indicating that the sample should not be contaminated by chance coincidences. The 7 selected objects are listed in Table 2. Fluxes at 1.4 GHz and spectral slopes were retrieved from Richards (2000) in 6 cases, and from Garrett (2000) in one case.

While rest-frame 0.5–2.0 and 2.0–10 keV luminosities could be obtained by K-correcting the observer's frame counts, this would imply the assumption of a spectral shape; but none of the seven deep field galaxies is individually detected in the hard band, so that any constraint on their spectra obtained with the use of a hardness ratio diagram is too loose to be significant (Fig. 4). However this problem may be partially circumvented by resizing the X-ray bands in the observer's frame according to the redshift of the objects. It is therefore possible to give better constraints to the spectrum of the deep field galaxies and derive better estimates of their luminosities.

Thus we redefine the soft and hard[3] bands as the $[0.5; 2.0/(1 + z)]$ and $[2.0/(1 + z); 10/(1 + z)]$ intervals, respectively.

---

[3] Since *Chandra* has very poor sensitivity between 8 and 10 keV, the use of the reduced 2–8 keV band enhances the signal/noise ratio. Note that while counts are extracted in the 2–8 keV band, fluxes and luminosities are always extrapolated to the 2–10 keV band.

Another advantage of this procedure is that the higher the redshift, the more akin the new hard band is to the zone of maximum sensitivity of *Chandra* (∼1–4 keV). Note that since the ACIS-I detector has almost no sensitivity below 0.5 keV, we fixed this energy as the lower limit for count extraction. For the two highest redshift galaxies, this reduces the soft band to 0.5–0.9 keV, still significantly larger than the ACIS-I energy resolution ($FWHM \lesssim 100$ eV).

We extracted counts in circular regions around our selected targets (radius 5 pixels); background was taken in annuli surrounding the targets. The net counts did not show dependence on the choice of background regions; they were converted in count rates with the exposure times listed in the Brandt et al. (2001) catalogue. Counts and rates are reported in Table 3. Best-fit slopes reproducing the soft/hard count ratio were derived by assuming a power-law spectrum with Galactic absorption. We find that six objects have spectral slopes falling in the range $\Gamma \sim 1.5$–2.7 (Table 3). To check whether these spectra are consistent with those of the galaxies in the local sample we calculated the observed soft/hard flux ratio for galaxies in the local sample: the median value for this flux ratio is 0.95 leading to a slope $\Gamma \sim 2.1$. The count ratios for each of the six deep field galaxies are consistent within 1–2σ with the $\Gamma \sim 2.1$ slope. The remaining source (#194 in Table 3, at $z = 1.275$) has an upper limit on the soft X-ray counts and a count ratio not consistent at the 5σ level with the unabsorbed $\Gamma \sim 2.1$ spectrum: it requires an inverted spectrum ($\Gamma < 0.1$) if no absorption is assumed, otherwise, if we assume $\Gamma = 2.1$, the intrinsic absorbing column has to be $N_H \gtrsim 3.4 \times 10^{22}$ cm^{-2}.

With the best-fit slopes we derived soft and hard band fluxes and luminosities (Fig. 5). The linear radio/X-ray correlations hold also for the Deep Field galaxies; the dispersion of the relations given in Sect. 3 is not changed by the inclusion of the deep field objects. A similar relation was also found in a recent paper by Bauer et al. (2002).

6. X-ray number counts and background

An estimate of the contribution of star-forming galaxies to the cosmic X-ray background (XRB) has been attempted several times (e.g. Bookbinder et al. 1980; Griffiths & Padovani 1990; Moran et al. 1999). The main purpose for the earlier studies was the possibility to explain the flatness of the XRB spectrum via the X-ray binaries powering the X-ray emission of these galaxies. Although AGN have since been recognized to provide by far the most important contribution to the XRB (Setti & Woltjer 1989; Comastri et al. 1995), the ongoing deep *Chandra* and XMM-*Newton* surveys offer unique opportunities to both test the AGN models and pin down the contribution from other kind of sources. Here, making use of the X-ray/radio relationships of Sect. 3, we perform an estimate of the contribution to the XRB by star-forming galaxies.

We consider the radio sub-mJy population associated with faint blue galaxies at high redshifts ($22 \lesssim V \lesssim 27$, $0.5 \lesssim z \lesssim 1.5$; Windhorst et al. 1990) representing an early era of star formation in the universe (Haarsma et al. 2000). This strongly evolving population accounts for the majority of the number counts below ∼0.5 mJy (Windhorst et al. 1985) and
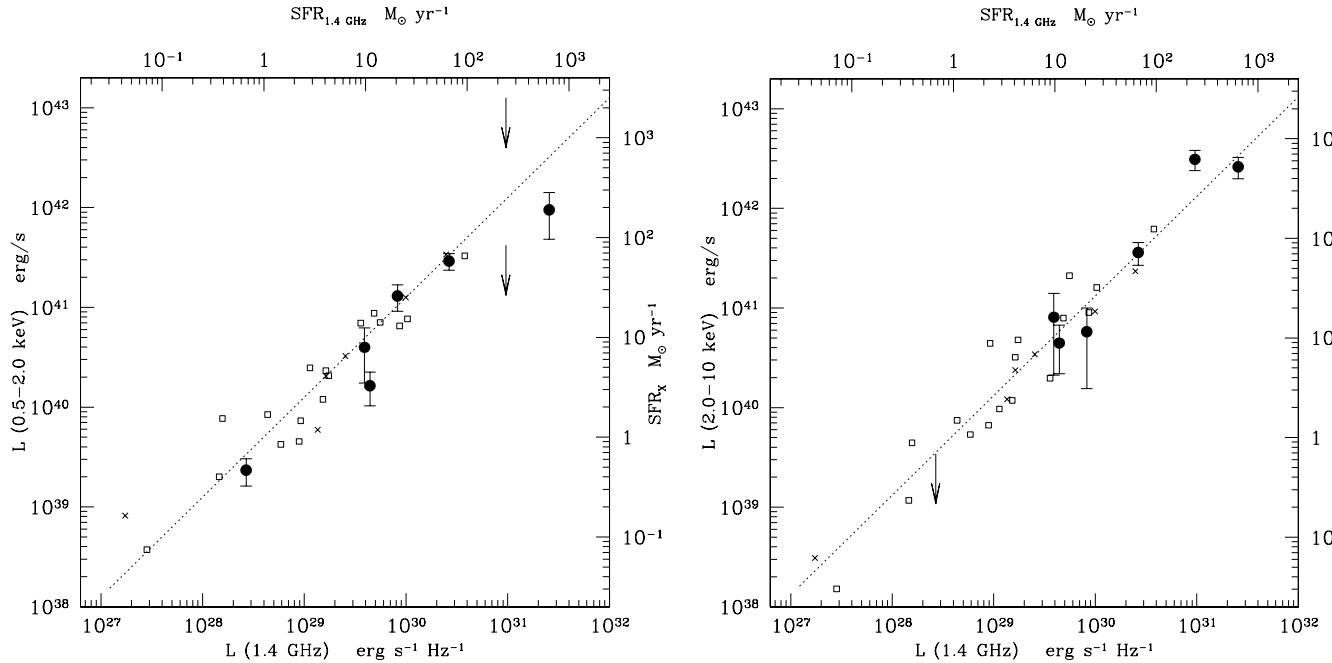
Fig. 5. The radio/X-ray luminosity relation for galaxies in the Hubble Deep Field (filled circles). Open squares and crosses: local galaxies as in Fig. (1); dotted lines: linear fits for local galaxies (Eq. (9)). The two most luminous galaxies are at $z = 1.275$ and 1.219 in order of increasing radio luminosity. The two upper limits (3σ level) in the left panel refer to source #194 (see text) and show the unabsorbed luminosity as estimated with $\Gamma \sim 0.1$ and no intrinsic absorption (lower) and with $\Gamma \sim 2.1$ and $N_H \sim 3.4 \times 10^{22}$ cm^{-1} (upper).

contribute about half of the radio cosmic background at 1.4 GHz (Haarsma et al. 2000). The deepest radio surveys have been performed at 1.4 GHz (Richards 2000), 5 GHz (Fomalont et al. 1991) and 8.4 GHz (Richards et al. 1998). Although a quick estimate of the contribution to the XRB may be worked out by simply applying Eqs. (9), (13) to the total radio fluxes obtained by integrating over the deepest radio Log N–Log S, it is instructive to first derive the X-ray source counts and compare them with the deepest counts obtained by *Chandra*. In order to derive the X-ray counts from the radio ones a full knowledge of the redshift distribution and spectra of the sources would be required. Under the simplifying assumption that the sub-mJy population lies at a redshift $\bar{z}$, so that the K-correction term is the same for all sources, the differential counts are obtained as:

$$n(S_X) = n(S_{1.4} \cdot \kappa^X_{1.4}) \tag{16}$$

where $n(S)$ are the differential number counts, and $\kappa^X_{1.4} = \kappa^X_{1.4}(\bar{z}, \alpha, \Gamma)$ is the X-ray band/1.4 GHz luminosity ratio (Eqs. (9), (13)) which depends on the redshift and on the radio and X-ray spectral indices via the K-correction:

$$\kappa^X_{1.4}(\bar{z}, \alpha, \Gamma) = \kappa^X_{1.4}\big|_{z=0} \cdot (1 + \bar{z})^{-(\Gamma-1)+\alpha}. \tag{17}$$

Concerning the sub-mJy Log N–Log S, Richards (2000) gives $n(S) = (2.51 \pm 0.13) \times 10^{-3} S^{-2.38 \pm 0.13}$ deg^{-2} Jy^{-1} as a best-fit to the differential number counts at 1.4 GHz in the range 45–1000, while Fomalont et al. (1991) find $n(S) = 1.2 \times 10^{-3} S^{-2.18 \pm 0.19}$ at 5 GHZ in the range 16–1500 μJy. The number density at 4 μJy (as estimated from fluctuation analysis) is consistent with extrapolation of the 16–1500 μJy slope.

The mean radio spectral index is in the range $\alpha = 0.3$–0.7. Fomalont et al. (1991) report their distribution as having

a moda of $\alpha = 0.5$, a median of $\alpha = 0.38$, and an average of $\alpha = 0.28$ (indices measured between 1.5 and 5 GHz). From Richards (2000) data we find an average $\alpha = 0.47$ (between 1.4 and 8.4 GHz), when we consider detections at both frequencies, and $\alpha = 0.67$ when we consider only detections at 1.4 GHz and treat upper-limits at 8.4 GHz as detections. The latter, steeper slope is also more consistent with the average index of our HDFN sample (Table 3). Here we assume $\alpha = 0.5$, and estimate the uncertainty in the K-correction due to the radio spectral index to be around a 15−20%.

According to the results of Sect. 5, we further assume an average X-ray spectral slope $\Gamma = 2.1$. For the sake of simplicity we also assume that the objects are placed at $\bar{z} \sim 1$, the mean redshift for the sub-mJy galaxies which, according to Windhorst et al. (1990), are distributed in the redshift interval 0.5–1.5 with a peak at $z \sim 1$. To estimate the effect on the counts due to the actual distribution of the sources in this redshift interval we consider a simplified case in which they are equally distributed at redshifts $z = 0.5$, 1.0 and 1.5. Since the effect enters in the computations via the K-correction term, we find that the predicted number counts would increase by only $\sim$10%. As a last remark we notice that a fraction, as yet undefined, of the X-ray spectra might steepen at energies $\gtrsim$10 keV, thus entailing a decrease in the predicted source counts; however, given the redshift range under consideration, the predicted soft X-ray source counts should not be affected.

The X-ray number counts predicted with the above assumptions (i.e. $\alpha = 0.5$, $\Gamma = 2.1$) from Richards (2000) and Fomalont et al. (1991) Log N–Log S are shown in Fig. 6, along with observed counts from Brandt et al. (2001), limits from fluctuation analysis (Miyaji & Griffiths 2002a,b) and predicted

Table 3. Data for deep field galaxies (counts, fluxes, luminosities). Γ is the best fit X-ray slope (photon index), α the radio slope (energy index). Sources are identified via their entry number in the Brandt et al. (2001) catalogue (cf. Table 2). X-ray fluxes in 10^{-17} erg s^{-1} cm^{-2}, radio fluxes in μJy. X-ray luminosities in 10^{40} erg s^{-1}, radio luminosities in 10^{30} erg s^{-1} Hz^{-1}. X-ray counts are extracted in redshifted bands (soft band := 0.5–2.0/$(1+z)$ keV, hard band := 2.0/$(1+z)$–8/$(1+z)$ keV). X-ray fluxes and luminosities are in rest-frame 0.5–2.0 and 2.0–10 keV bands, radio ones at rest-frame 1.4 GHz. For source #194, the absorbed flux and luminosity are quoted. The unabsorbed luminosity is $\lesssim 4 \times 10^{42}$ erg s^{-1}.

|		FLUXES AND LUMINOSITIES: DEEP SAMPLE									
		SOFT X-RAYS			HARD X-RAYS				RADIO		
SOURCE	z	COUNTS	F	L	COUNTS	F	L	Γ	F	L	α
134	0.456	31 ± 6	23	29	22 ± 6	28	36	$2.0^{+0.4}_{-0.3}$	210	2.6	0.7
136	1.219	5.9 ± 3	6.7	95	22 ± 5	19	260	$1.6^{+0.9}_{-0.5}$	180	26	0.7
148	0.078	14 ± 4	8.4	0.23	<2.1	<4.1	<0.11	>2.6	96	0.027	0.6
188	0.410	15 ± 4	13	13	5.2 ± 4	5.8	5.8	$2.7^{+1.5}_{-0.6}$	83	0.82	0.6
194	1.275	<1.6	<0.88	<14	23 ± 5	20	310	<0	60	9.6	0.9
246	0.423	6.2 ± 4	3.7	4.0	5.4 ± 4	7.5	8.1	$1.7^{+1.4}_{-0.6}$	36	0.39	0.4
278	0.232	11 ± 4	5.8	1.6	7.8 ± 4	16	4.4	$1.5^{+0.7}_{-0.4}$	160	0.44	0.2
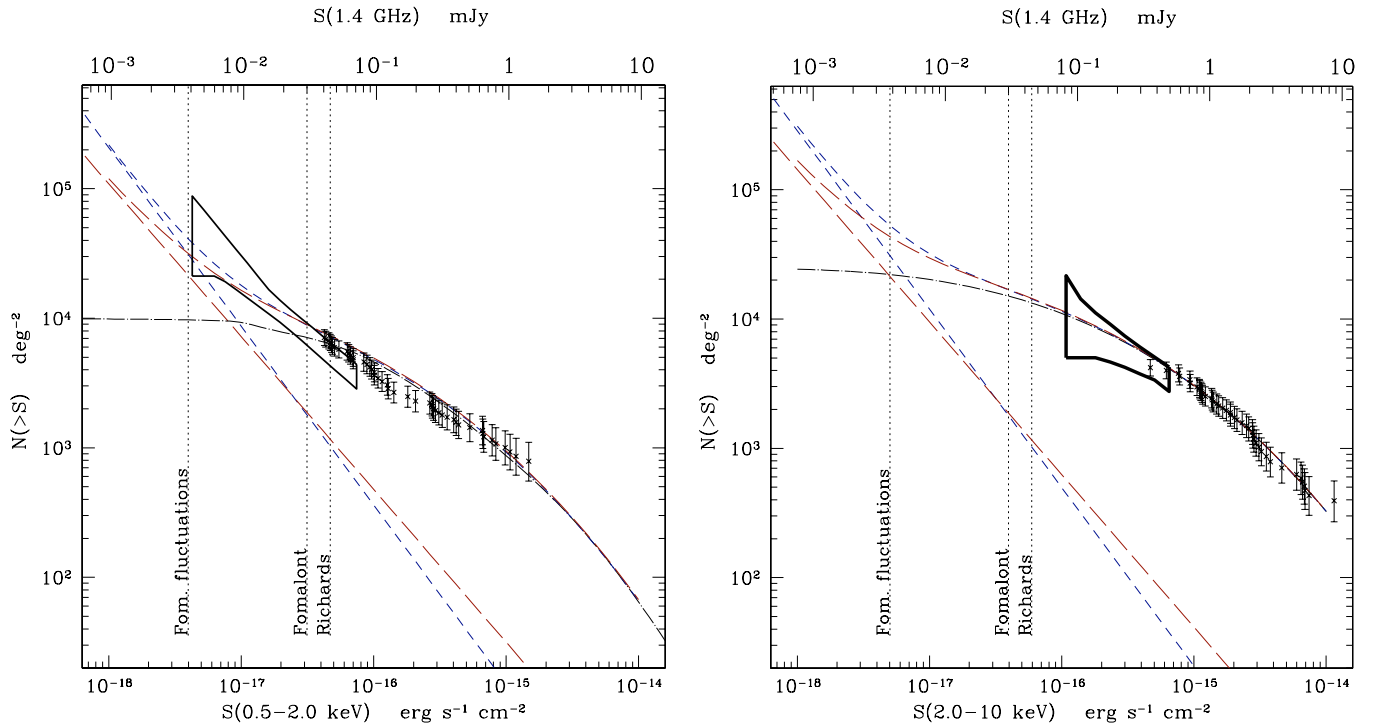
Fig. 6. X-ray counts derived from deep radio Log N–Log S. The short-dashed lines represent the 1.4 GHz Log N–Log S (Richards 2000) with K-corrections assuming $\bar{z} = 1$, $\Gamma = 2.1$ and $\alpha = 0.5$. The long-dashed lines represent the Log N–Log S by Fomalont et al. (1991) reported at 1.4 GHz with $\alpha = 0.5$ (K-corrections like for the 1.4 GHz one). The dots are the observed X-ray number counts in the HDFN (Brandt et al. 2001); while the horn-shaped symbols show the results from X-ray fluctuation analysis (Miyaji & Griffiths 2002a,b). The dot-dashed line shows the number counts from AGN synthesis models (Comastri et al. 1995). The vertical dotted lines show the limiting sensitivities for the radio surveys. The total of AGN plus galaxy counts predicted from the radio counts of Richards (2000) and Fomalont et al. (1991) are also shown with short and long dashed lines, respectively.

counts from AGN synthesis models (Comastri et al. 1995). The latter are essentially in agreement with the results of more recent synthesis models (Gilli et al. 2001). The extrapolations of the radio Log N–Log S below $\sim$50 μJy and down to a few μJy at 1.4 GHz ($\sim$6 $\times$ 10^{-18} erg s^{-1} cm^{-2} in the 0.5–2.0 keV band) are consistent with the limits from fluctuation analysis (Miyaji & Griffiths 2002b) and do not exceed the X-ray expected number counts. Since Miyaji & Griffiths (2002b) suggested the emergence of a new population (beyond that of AGN which

dominates at brighter fluxes) in the 0.5–2.0 keV band at fluxes around 10^{-17} erg s^{-1} cm^{-2}, it is tempting to identify this new population with the sub-mJy galaxies. It should be noted, however, that Eqs. (9), (13) may not apply to the entire sub-mJy population. For instance, a fraction (up to a 15–20%, Haarsma et al. 2000) of the sources may still present a dominant contribution from an AGN. It follows that the derived Log N–Log S should be regarded as an upper limit to the X-ray counts from star-forming galaxies.

As a final remark it should be pointed out that our results depend on the basic assumption of a strict linearity between the radio and X-ray luminosities. Had we assumed a non-linear relationship, such as Eq. (7) for the soft X-rays or Eq. (11) for the 2–10 keV band, we would have found an increase or decrease, respectively, of about 50% in the predicted counts at a flux level around 10^{-17} erg s^{-1} cm^{-2}. A larger, well defined sample of star-forming galaxies down to the faintest radio and X-ray fluxes would obviously be of great importance to better constrain the X-ray vs. radio luminosities relationship. It might be argued that a more direct derivation of the source counts could be made by adopting the observed fluxes, rather than the luminosities of the objects. However, this procedure would entail an arbitrary extrapolation of the X-ray/radio flux ratio for almost two orders of magnitude at fluxes fainter than the *Chandra* deep field. On the other hand, the radio luminosity interval of Fig. 5 essentially encompasses the radio power of the sub-mJy population if placed in the redshift interval mentioned above.

The derived X-ray number counts can be integrated to estimate the contribution to the XRB. For the observed 2–10 keV background we take the XMM-*Newton* value of 2.15×10^{-11} erg s^{-1} cm^{-2} (Lumb et al. 2002), which is comprised between the ASCA (Gendreau et al. 1995) and BeppoSAX (Vecchi et al. 1999) figures. The integration of counts derived from the 1.4 GHz Log N–Log S (Richards 2000), performed in its validity range (5.9×10^{-17}–1.3×10^{-15} erg s^{-1} cm^{-2}, corresponding to 45-1000 μJy at 1.4 GHz), yields a contribution to the XRB of 4.0×10^{-13} erg cm^{-2} s^{-1} ($\lesssim$2% of the observed background). By extrapolating to 10^{-18} erg s^{-1} cm^{-2} ($\sim$1 μJy) the contribution would increase to 2.3×10^{-12} erg cm^{-2} s^{-1} (11%). Integration of counts from the flatter Fomalont et al. (1991) Log N–Log S in the 1–1000 μJy range yields a contribution of 1.4×10^{-12} erg cm^{-2} s^{-1} (6.4%). We also note that 1 μJy at 1.4 GHz is a limit $\sim$3−5 times fainter than the constraint from radio fluctuation analysis; it is unlikely that the radio Log N–Log S could sustain its slope below this limit, otherwise the integrated radio emission from weak sources would diverge (Fomalont et al. 1991).

7. Conclusions

We have analyzed a small, but well defined sample of 17 star-forming galaxies, extracted from the HFS97 catalogue, for which there is a homogeneous information on optical, *FIR*, radio and X-ray bands (local sample). In agreement with previous work (David et al. 1992) we find that the logarithms of the soft (0.5–2 keV) X-ray luminosities (corrected for Galactic absorption only) are linearly correlated with the logarithms of both radio (1.4 GHz) and *FIR* luminosities. We have extended our analysis to the harder X-ray band, essentially free from internal absorption which may affect the soft X-ray fluxes, and found that there is a tight linear correlation between the X-ray luminosities in the 2–10 keV interval with both the radio and the *FIR* luminosities, normally assumed as the indicators of the star formation rate. The addition of 6 galaxies (supplementary sample) homogeneous with, but not included in HFS97, does not modify these results. We conclude that the origin of the

hard X-ray emission must be closely related to star formation and calibrate an X-ray *SFR* indicator.

Candidate starburst galaxies have been selected in the HDF North, with redshifts up to $z \sim 1.3$, and their rest-frame X-ray luminosities are computed by extracting counts in redshifted bands from the *Chandra* observation of the HDFN. With this approach we have shown that the 2–10 keV/radio linear correlation holds up to $z \sim 1.3$, encompassing five orders of magnitude in luminosity, up to $L_{2-10} \sim$ several 10^{42} erg s^{-1} and a corresponding star formation rate $\sim$1000 $M_\odot$ yr^{-1}. The fit to the 0.5–2.0 keV/radio data is also linear up to $z \sim 1.3$. However, the count ratio for the highest redshift galaxy at $z = 1.275$ requires significant absorption if a spectral slope of $\Gamma \sim 2.1$ is assumed; thus this galaxy shows, on a larger scale, the same behaviour as that of the southern core in NGC 3256 (see the appendix). Therefore, while the linearity of the relations involving soft X-ray luminosities remains statistically significant, at high redshift (where galaxies are supposed to have more gas at their disposal to form stars, and so their X-ray emission is more likely to be absorbed) the 2–10 keV luminosity is a more secure indicator of the *SFR*.

As an additional investigation we have also analyzed a sample of LLAGN (LINERs and Seyfert's) included in HFS97 (Terashima et al. 2002): while, as expected, the X-ray luminosities are generally in excess with respect to star-forming galaxies for the same *FIR* luminosity, the distribution of the objects in the X-ray vs. *FIR* luminosity diagram is bounded from below from the region occupied by the star-forming galaxies, indicating that the X-ray emission of LLAGN falling in this border-line region could be mainly due to star formation processes, rather than being of nuclear origin.

Our inference of using the 2–10 keV luminosity as a *SFR* indicator is consistent with a recent study on Lyman-break galaxies by Nandra et al. (2002) who have extrapolated the David et al. (1992) *FIR*/soft X-ray relation to the hard X-ray band obtaining a *SFR*/2–10 keV luminosity relation within 10% of our Eq. (15). From a stacking analysis of *Chandra* data for a sample of optically selected Lyman-break and Balmer-break galaxies in the HDFN they find a good agreement of the average *SFR* as estimated from X-ray and extinction-corrected UV luminosities.

Grimm et al. (2002) have recently claimed that the luminosity function of High Mass X-ray Binaries (HMXB) can be derived from a universal luminosity function whose normalization is proportional to the *SFR*, but only for rates $\gtrsim$1 $M_\odot$/yr, while this relation becomes non-linear at lower rates. This appears to be somewhat in contrast with our result that the 2–10 keV luminosity is proportional to *SFR* even for rates $\lesssim$1 $M_\odot$/yr, as supported by the data for 4 galaxies in our sample. However, Grimm et al. 2002 analysis only refers to the contribution from HMXB; the possible contribution of other X-ray components, which are not selected out in our data, might explain this discrepancy.

X-ray number counts for the radio sub-mJy galaxy population are predicted making use of the radio Log N–Log S and of the X-ray/radio correlation. The expected counts extend much below the sensitivities of the deepest X-ray surveys (about one order of magnitude in the soft band, one and a half for the hard

band), and are within the limits set by the fluctuations analysis in the *Chandra* deep fields (Miyaji & Griffiths 2002a, b). They are also consistent with the predictions based on the evolution of the cosmic *SFR* density by (Ptak et al. 2001). Since the results from fluctuations analysis in the soft X-rays suggest an excess of sources with respect to AGN synthesis models at fluxes below $\sim 10^{-17}$ erg s^{-1} cm^{-2}, it may be possible that the sub-mJy galaxies represent the dominant population in the X-rays at very faint fluxes.

The contribution to the cosmic X-ray background in the 2–10 keV band is estimated by integration of the derived X-ray number counts. The contribution from galaxies detected in the deepest radio surveys is ≲2%. This estimate may rise up to 11% by extrapolating the radio counts down to 1 μJy, or $\sim 10^{-18}$ erg s^{-1} cm^{-2} in the X-ray band. However, since a fraction of the sub-mJy objects may not be star-forming galaxies, these figures for the time being should be regarded as upper limits.

The next step in understanding the physics involved in hard X-ray emission must go through a careful analysis of *Chandra* and XMM-*Newton* observations of both low-*SFR* local galaxies and high-*SFR* high-redshift ones. Since the explanation of the radio/*FIR* correlation is still a matter of discussion, we hope that its extension to the X-ray band may help in clarifying this issue.

Appendix A: Notes on individual galaxies

IC 342: Variability of ULXs

In the ASCA observations, the X-ray emission of IC 342 (a face-on spiral galaxy at 3.9 Mpc) is powered by three main sources; two of them (source 1 and 2 according to Fabbiano & Trinchieri 1987) are ultraluminous X-ray binaries (ULX) while source 3 is associated with the galactic centre. Observations with higher angular resolution (ROSAT HRI, Bregman et al. 1993) showed that sources 1 and 2 are point-like while source 3 is resolved in at least three sources. Our main concern in determining the flux of this galaxy is the variability of the two ULX, which was assessed by a series of observations spanning several years: IC342 was first observed by *Einstein* in 1980 (Fabbiano & Trinchieri 1987), then by ROSAT in 1991 (Bregman et al. 1993), by ASCA in 1993 (Okada et al. 1998) and 2000 (Kubota et al. 2001), and by XMM-*Newton* in 2001.

In Table A.1 we report soft X-ray fluxes for sources 1 and 2. We have chosen the soft X-ray band due to the limited energy band of both *Einstein* and ROSAT; the fluxes observed with

Table A.1. 0.5–2.0 keV fluxes (in 10^{-13} erg s^{-1} cm^{-2}) for sources 1 and 2 in IC 342 for a blackbody (bb) and a power-law (po) model.

YEAR	MISSION	SRC 1 FLUX BB	SRC 1 FLUX PO	SRC 2 FLUX PO
1980	*Einstein*	2.7	4.1	0.85
1991	ROSAT	3.3	2.7	1.3
1993	ASCA	16		2.6
2000	ASCA		5.0	0.52
2001	XMM-*Newton*		4.1	1.3

these satellites were obtained from the count rates reported in Fabbiano & Trinchieri (1987) and Bregman et al. (1993) assuming the powerlaw and multicolor disk examined in Kubota et al. (2001) for source 1 and 2 respectively; we take ASCA 1993 and 2000 fluxes from Kubota et al. (2001). XMM-*Newton* archival observations were reduced by us with SAS 5.3 and the latest calibrations available.

Source 1 was in a low state ($F_{0.5-2} \sim 3$–5×10^{-13} erg s^{-1}) during the 1980, 1991, 2000 and 2001 observations, and in a high state ($F_{0.5-2} \sim 16 \times 10^{-13}$ erg s^{-1}) during the 1993 observation. The broad-band (0.5–10 keV) spectrum changed, its best-fit model being a disk black-body in 1993 and a power-law in 2000 and 2001. Source 2 has also shown variability, its 0.5–2.0 keV flux oscillating between 0.52×10^{-13} (ASCA 2000) and 2.56×10^{-13} (ASCA 1993) erg s^{-1}; the main reason for this variability being the variations in the strongly absorbing column density, which was 9.9×10^{21} cm^{-2} in 1993 and 18×10^{21} cm^{-2} in 2000. The spectrum was always a power-law.

The high state for source 1 seems thus to be of short duration, and we feel confident that its time-averaged flux may be approximated with its low state flux. We thus choose to derive our flux estimate for IC 342 from the ASCA 2000 observation, estimating the variation for the total flux of the galaxy caused by source 2 variability to be less than 10%.

Variability in M 82

Hard (2–10 keV) X-ray variability in M 82 was reported in two monitoring campaigns with ASCA (in 1996, Ptak & Griffiths 1999) and RXTE (in 1997, Rephaeli & Gruber 2002). M82 was found in "high state" (i.e. $4 \times 10^{-11} \lesssim f_{2-10} \lesssim 7 \times 10^{-11}$) in three out of nine observations with ASCA and in 4 out of 31 observations with RXTE. In all the other observations it was in a "low state" ($2 \times 10^{-11} \lesssim f_{2-10} \lesssim 3.5 \times 10^{-11}$). A low flux level was also measured during the observations with other experiments: HEAO 1 in 1978 (Griffiths et al. 1979); *Einstein* MPC in 1979 (Watson et al. 1984); EXOSAT in 1983 and 1984; BBXRT in 1990; ASCA in 1993 (Tsuru et al. 1997); BeppoSAX in 1997 (Cappi et al. 1999); *Chandra* in 1999 and 2000, XMM-*Newton* in 2001. No variability was instead detected in the 0.5–2.0 keV band (Ptak & Griffiths 1999).

The high state has been of short duration: less than 50 days in 1996, when it was observed by ASCA, and less than four months in 1997. A monitoring campaign was also undertaken with *Chandra*, which observed M 82 four times between September 1999 and May 2000. We reduced the archival data,
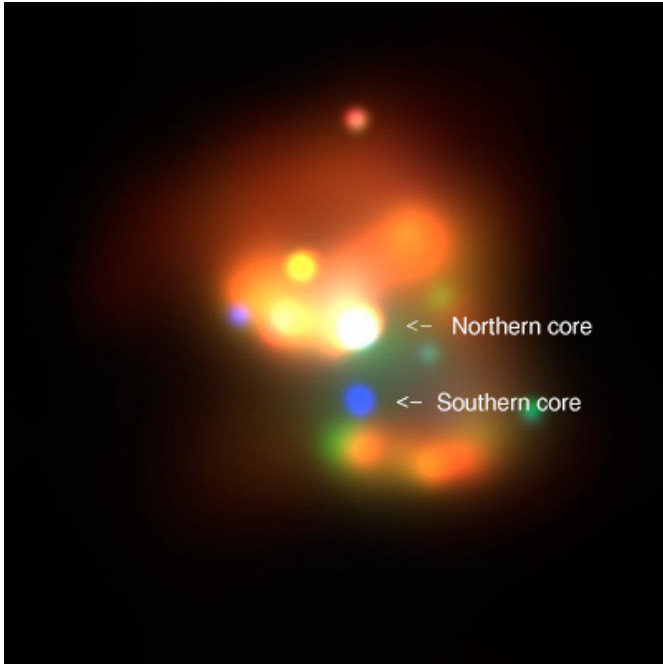
Fig. A.1. True color, smoothed *Chandra* image of the centre of NGC 3256 (the actual colour is the sum of red, green and blue, the intensity of each one representing the flux in the 0.3–1.0 keV, 1.0–2.0 keV and 2.0–8 keV respectively); north is up, east is left; the distance between the two cores is ~5″. The two cores are the brightest sources both at 1.4 GHz and in the 2–10 keV band, but since the southern one lies behind a dust lane, its soft X-ray emission is completely absorbed. While the northern core follows both the radio/soft X-ray and radio/hard X-ray relations (Eqs. (9), (13)), the southern one only follows the radio/hard X-ray relation.

and found that the galaxy was always in a low state, with its flux slowly increasing from 1.2×10^{-11} to 2.9×10^{-11}.

We do not attempt a detailed analysis of the variability (see Rephaeli & Gruber 2002); however, we feel confident that, given the short duration of the high states and the fact that the difference between high- and low state flux is about a factor 2, the time-averaged flux of M 82 can be approximated with its low state flux. We thus choose to derive our flux estimate for M 82 from the BeppoSAX 1997 observation ($f_{2-10} = 2.9 \times 10^{-11}$ erg s^{-1} cm^{-2}), estimating the uncertainty caused by variability to be around 30%.

NGC 3256: A case for intrinsic absorption

We present the test case of NGC 3256, a luminous dusty merger remnant included in the supplementary sample. Detailed studies at several wavelengths (radio: Norris & Forbes 1995; IR: Kotilainen et al. 1996; optical: Lípari et al. 2000; X-ray: Moran et al. 1999; Lira et al. 1999) have shown that the energetic output of this galaxy is powered by star formation occurring at several locations, but mainly in the two radio cores discovered by Norris & Forbes (1995) and also detected with *Chandra* (Fig. A.1).

The 3 and 6 cm radio maps (Norris & Forbes 1995) reveal two distinct, resolved ($FWHM \sim 1.2''$) nuclei and some

fainter diffuse radio emission. Separated by 5″ in declination, the two cores dominate the radio emission, the northern one being slightly (15%) brighter. They share the same spectral index ($\alpha \sim 0.8$) and have similar 2–10 keV fluxes. Both of them follow the radio/hard X-ray correlation, while only the northern one follows the radio/soft X-ray correlation. At other wavelengths the northern core is the brightest source in NGC 3256, while the southern one lies behind a dust lane and is only detected in the far infrared ($\lambda > 10 \ \mu$m), as clearly shown in the sequence of infrared images at increasing wavelengths in Kotilainen et al. (1996).

Although the southern core appears as a bright source in the hard X-rays ($E > 2$ keV), there are not enough counts to allow an accurate spectral fitting. However, it is still possible to constrain the absorbing column density by assuming a template spectrum, such as a simple power-law or the spectrum of the northern core, leading (after standard processing of the *Chandra* archival observation of NGC 3256) to an intrinsic $N_H = (2.2 \pm 1.0) \times 10^{22}$ cm^{-2} ($N_{H,Gal} = 9.5 \times 10^{20}$ cm^{-2}), fully consistent with the $A_V = 10.7$ estimated by Kotilainen et al. (1996) from infrared observations. We note that 84% of the 2–10 keV flux and only 10% of the 0.5–2 keV one are transmitted through this column density. Thus, while the flux loss in the hard band is still within the correlation scatter, the larger loss in the soft band throws the southern nucleus off the correlation of Eq. (9).

References

Bookbinder, J., Cowie, L. L., Ostriker, J. P., Krolik, J. H., & Rees, M. 1980, ApJ, 237, 647
Bauer, F. E., Alexander, D. M., Brandt, W. N., et al. 2002, AJ, 124, 2351
Brandt, W. N., Alexander, D. M., Hornschmeier, A. E., et al. 2001, AJ, 122, 2810
Bregman, J. N., Cox, C. V., & Tomisaka, K. 1993, ApJ, 415, L79
Cappi, M., Persic, M., Bassani, L., et al. 1999, A&A, 350, 777
Cohen, J., Hogg, D. W., Blandford, R., et al. 2000, ApJ, 538, 29
Comastri, A., Setti, G., Zamorani, G., & Hasinger, G. 1995, A&A, 296, 1
Condon, J. J. 1992, ARA&A, 30, 575
Condon, J. J., Helou, G., Sanders, D. B., & Soifer, B. T. 1990, ApJS, 73, 359
Condon, J. J., Helou, G., Sanders, D. B., & Soifer, B. T. 1996, ApJS, 103, 81
Dahlem, M., Weaver, K. A., & Heckman, T. M. 1998, ApJS, 118, 401
David, L. P., Jones, C., & Forman, W. 1992, ApJ, 388, 82
Della Ceca, R., Griffiths, R. E., Heckman, T. M., & MacKenty, J. W. 1996, ApJ, 469, 662
Della Ceca, R., Griffiths, R. E., & Heckman, T. M. 1997, ApJ, 485, 581
Della Ceca, R., Griffiths, R. E., Heckman, T. M., Lehnert, M. D., & Weaver, K. A. 1999, ApJ, 514, 772
De Jong, T., Klein, U., Wielebinski, R., & Wunderlich, E. 1985, A&A, 147, L6
de Vaucouleurs, G., de Vaucouleurs, A., & Corwin, H. G. 1976, Second Reference Catalogue of Bright Galaxies (University of Texas Press, Austin) (RC2)
Dobrodiy, O. A., & Pronik, I. I. 1979, Izv. Astrof. Obs. Krim. (Simeis) LX, 66
Fabbiano, G. 1989, ARA&A, 27, 87

Fabbiano, G., & Trinchieri, G. 1987, ApJ, 315, 46

Fomalont, E. B., Windhorst, R. A., Kristian, J. A., & Kellerman, K. I. 1991, AJ, 102, 1258

Garrett, M. 2002, A&A, 384, L19

Garrett, M. A., de Bruyn, A. G., Giroletti, M., Baan, W. A., & Schilizzi, R. T. 2000, A&A, 361, L41

Gendreau, K. C., Mushotzky, R., Fabian, A. C., et al. 1995, PASJ, 47, L5

Gilli, R., Salvati, M., & Hasinger, G. 2001, A&A, 366, 407

Griffiths, R. E., Schwartz, D. A., Schwarz, J., et al. 1979, ApJ, 230, L21

Griffiths, R. E., & Padovani, P. 1990, ApJ, 360, 483

Grimm, H. J., Gilfanov, M., & Sunyaev, R. 2002, MNRAS, submitted [astro-ph/0205371]

Haarsma, D. B., Partridge, R. B., Windhorst, R. A., & Richards, E. A. 2000, ApJ, 544, 641

Harwit, M., & Pacini, F. 1975, ApJ, 200, L127

Haynes, R. F., Huchtmeir, W. K. G., & Siegman, B. C. 1975, Compendium of Radio Measurements of Bright Galaxies, CSIRO Publication

Helou, G., Soifer, B. T., & Rowan-Robinson, M. 1985, ApJ, 298, L7

Ho, L. C., Filippenko, A. V., & Sargent, W. L. W. 1995, ApJS, 98, 477

Ho, L. C., Filippenko, A. V., & Sargent, W. L. W. 1997, ApJS, 112, 315 (HFS97)

Ho, L. C., Feigelson, E. D., Townsley, L. K., et al. 2001, ApJ, 549, L51

Kennicutt, R. C. Jr. 1998, ApJ, 498, 541

Kewley, L. J., Heisler, C. A., Dopita, M. A., & Lumsden, S. 2001, ApJS, 132, 37

Kotilainen, J. K., Moorwood, A. F. M., Ward, M. J., & Forbes, D. A. 1996, A&A, 305, 107

Kubota, A., Mizuno, T., Makishima, K., et al. 2001, ApJ, 547, L119

Lípari, S., Díaz, R., Taniguchi, Y., et al. 2000, AJ, 120, 645

Lira, P., Ward, M., Zezas, A., Alonso-Herrero, A., & Ueno, S. 2002, MNRAS, 330, 259

Lumb, D. H., Warwick, R. S., Page, M., & De Luca, A. 2002, A&A, 389, 93

Mazzarella, J., et al. 2002, in preparation

Miyaji, T., & Griffiths, R. E. 2002a, ApJ, 564, L5

Miyaji, T., & Griffiths, R. E. 2002b, Proc. Symp., New Visions of the X-ray Universe in the XMM-Newton and Chandra Era, ESTEC 2001 [astro-ph/0202048]

Moran, E. C., Lehnert, M. D., & Helfand, D. J. 1999, ApJ, 526, 649

Moshir, M., Copan, G., Conrow, T., et al. 1989, IRAS Faint Source Catalog, |b| > 10 Degrees, Infrared Processing and Analysis Center

Nandra, K., Mushotzky, R. F., Arnaud, K., et al. 2002, ApJ, 576, 625

Norris, R. P., & Forbes, D. A. 1995, ApJ, 446, 594

Okada, K., Dotani, T., Makishima, K., Mitsuda, K., & Mihara, T. 1998, PASJ, 50, 25

Ochsenbein, F., Bauer, P., & Marcout, J. 2000, A&AS, 143, 23

Parmar, A. N., Sidoli, L., Oosterbroek, T., et al. 2001, A&A, 368, 420

Ptak, A., & Griffiths, R. 1999, ApJ, 517, L85

Ptak, A., Griffiths, R., White, N., & Ghosh, P. 2001, ApJ, 559, L91

Ranalli, P., Comastri, A., & Setti, G. 2002, Proc. Symp., New Visions of the X-ray Universe in the XMM-Newton and Chandra Era, ESTEC 2001 [astro-ph/0202241]

Rephaeli, Y., & Gruber, D. 2002, A&A, 389, 752

Rice, W., Lonsdale, C. J., Soifer, B. T., et al. 1988, ApJS, 68, 91

Richards, E. A., Kellermann, K. I., Fomalont, E. B., Windhorst, R. A., & Partridge, R. B. 1998, AJ, 116, 1039

Richards, E. A. 2000, ApJ, 533, 611

Rubin, V. C., Ford, W. K. Jr., & D'Odorico, S. 1970, ApJ, 160, 801

Rush, B., Malkan, M., & Spinoglio, L. 1993, ApJS, 89, 1

Sandage, A. R., & Tammann, G. A. 1981, A Revised Shapley-Ames Catalog of Bright Galaxies (RSA) (Washington: Carnegie Institution of Washington)

Sansom, A. E., Dotani, T., Okada, K., Yamashita, A., & Fabbiano, G. 1996, MNRAS, 281, 48

Setti, G., & Woltjer, L. 1989, A&A, 224, L21

Terashima, Y., Iyomoto, N., Ho, L. C., & Ptak, A. F. 2002, ApJS, 139, 1

Tully, R. B. 1988, Nearby Galaxies Catalog (Cambridge University Press)

Tsuru, T. G., Awaki, H., Koyama, K., & Ptak, A. F. 1997, PASJ, 49, 619

Ulvestad, J. S., & Ho, L. C. 2002, ApJ, in press [astro-ph/0208460]

van der Kruit, P. C. 1973, A&A, 29, 263

Vecchi, A., Molendi, S., Guainazzi, M., Fiore, F., & Parmar, A. N. 1999, A&A, 349, L73

Veilleux, S., & Osterbrock, D. E. 1987, ApJS, 63, 295

Watson, M. G., Stanger, V., & Griffiths, R. E. 1984, ApJ, 286, 144

Webster, B. L., & Smith, M. G. 1983, MNRAS, 204, 743

Windhorst, R. A., Miley, G. K., Owen, F. N., Kron, R. G., & Koo, D. C. 1985, ApJ, 289, 494

Windhorst, R. A., Mathis, D. F., & Neuschaefer, L. W. 1990, Proc. Symp., Evolution of the universe of galaxies: Edwin Hubble Centennial Symposium, ASP Conf. Ser., 10, 389

Yun, M. S., Reddy, N. A., & Condon, J. J. 2001, ApJ, 554, 803

Zezas, A. L., Georgantopoulos, I., & Ward, M. J. 1998, MNRAS, 301, 915